

# Stimulated radar collider for testing a model of dark energy

Kensuke Homma<sup>1,\*</sup> and Yuri Kirita<sup>1</sup>

<sup>1</sup>*Graduate School of Science, Hiroshima University,  
Kagamiyama, Higashi-Hiroshima, Hiroshima 739-8526, Japan*

(Dated: November 19, 2019)

We propose a stimulated pulsed-radar collider for testing a dilaton model with the mass of  $\sim 10^{-7}$  eV as a candidate of dark energy. We have extended formulae for stimulated resonant photon-photon scattering in a quasi-parallel collision system by including fully asymmetric collision cases. With a pulse energy of 100 J in the GHz-band, for instance, which is already achieved by an existing klystron, we expect that the sensitivity can reach gravitationally weak coupling domains, if two key technological issues are resolved: pulse compression in time reaching the Fourier transform limit, and single-photon counting for GHz-band photons. Such testing might extend the present horizon of particle physics.

## 1. INTRODUCTION

Since Rutherford's experiment, the observation of quantum scattering processes caused by colliding energetic charged particles has unveiled deeper layers of nature at the microscopic. With knowledge gleaned from these particle collisions, the Standard Model (SM) of elementary particles is now almost confirmed, with the recent discovery of the Higgs boson providing another point of evidence for the SM. However, the SM is still unsatisfactory when trying to quantitatively understand the profile of the energy density of the universe as evaluated from macroscopic gravitational observables through curvatures in spacetime. In particular, the SM can explain only  $\sim 5\%$  of the observed energy density of the universe. The remainder of the energy density is assumed to be accounted for by dark matter and dark energy [1]. Why, then, is so little understood about dark components?

The gravitational coupling strength  $G_N \sim 10^{-38} \text{ GeV}^{-2}$  ( $\hbar = c = 1$ ) is extraordinary weak, even relative to the weakest coupling strength of the weak interaction  $G_F \sim 10^{-5} \text{ GeV}^{-2}$  among the SM. Because of its extraordinary weakness, gravitational coupling has never been probed by elementary scattering processes. In this sense, gravity has been, in practice, beyond the scope of experimental particle physics to date. Therefore, it is unlikely that present knowledge of particle physics is sufficient to understand dark components obtained from gravitational observables. We suggest in this paper that we can actually test scattering processes, even with gravitationally weak coupling, if a properly designed stimulated photon-photon collider is used. Such testing might extend the present horizon of particle physics.

Massless Nambu-Goldstone fields accompany spontaneous breaking of global continuous symmetries [2]. The neutral pion is a typical Nambu-Goldstone Boson (NGB). However, the physical mass is slightly greater

than zero. This pseudo-NGB (pNGB) state is caused by chiral symmetry breaking in quantum chromodynamics (QCD). However, pNGBs are not limited to chiral symmetry. In general, whenever a global symmetry of any type is broken, we may expect a pNGB to exist. This viewpoint can be used as a robust guiding principle to search for something very low in mass in the Universe, even without knowing the details of individual dynamics.

In this paper, we focus on a dilaton field [3] as a pNGB caused by breaking of dilatation (scale) symmetry for which fifth-force searches have been stimulated [4]. This dilaton field can be a testable source of dark energy in laboratory experiments. The discovery of an accelerating universe revived today's version of the cosmological constant, leaving fine-tuning and coincidence problems unresolved. The simplest known approach to explain these problems is to introduce a scalar field, the dilaton. Fujii proposed a scalar-tensor theory with a cosmological constant  $\Lambda$  (STTL) [5] based on Jordan's scalar-tensor theory (STT) [6], one of the best-known alternatives to Einstein's General Relativity. STTL yields the scenario of a decaying cosmological constant in the Einstein frame corresponding to the observational frame resulting in  $\Lambda_{\text{obs}} \sim t^{-2}$ , where the present age of the universe,  $t_0 = 1.37 \times 10^{10} \text{ y}$ , is re-expressed as  $\sim 10^{60}$  in the reduced Planckian units with  $c = \hbar = M_{\text{P}} (= (8\pi G)^{-1/2} \sim 10^{18} \text{ GeV}) = 1$ . Given the unification-oriented expectation  $\Lambda \sim 1$  in these units, the decay behavior provides us a natural way of understanding why the observed value may be as small as  $10^{-120}$ . As of this writing, the most up-to-date evaluation of the gravitationally coupling dilaton mass in STTL is  $(0.15 \sim 0.59) \times 10^{-6} \text{ eV}$ , based on the self-energy correction via Higgs two-loop diagrams [7].

To directly probe this low-mass dilaton field, photon-photon scattering has special advantages arising from the coupling of two photons, because photons are massless and the center-of-mass system (cms) energy,  $E_{\text{cms}}$ , can be extremely low in comparison with that of charged particle collisions. We therefore discuss the following effective Lagrangian, which expresses coupling to two photons:

$$-\mathcal{L} = gM^{-1} \frac{1}{4} F_{\mu\nu} F^{\mu\nu} \phi, \quad (1.1)$$

\*corresponding author: khomma@hiroshima-u.ac.jp

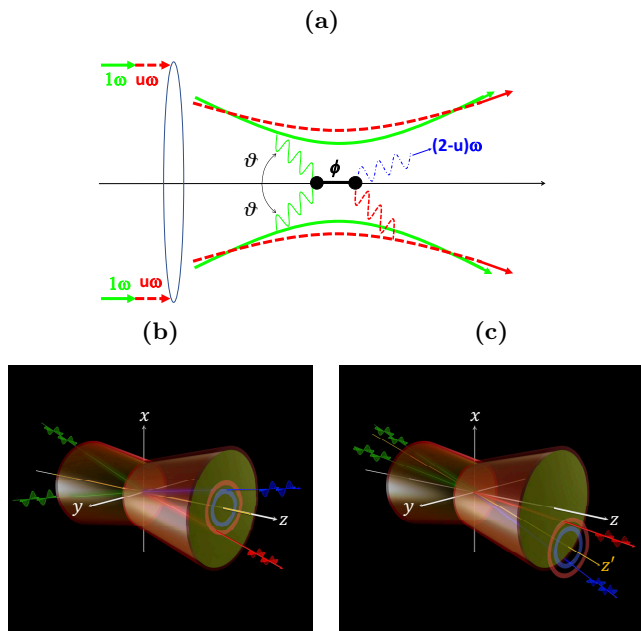


**FIG. 1:** Stimulated resonant scattering in a quasi-parallel collision system (QPS) and the classification of collision geometries. (a) Conceptual drawing of stimulated resonant photon–photon scattering in QPS, realizable when a coherent field with energy  $\omega$  (solid green line) is combined with another coherent field with energy  $u\omega$  ( $0 < u < 1$ ) (dashed red line) and both fields are focused by a lens element in vacuum. The emission of signal photons with energy  $(2 - u)\omega$  (dash-dotted blue line) is stimulated as a result of energy-momentum conservation in the scattering process  $\omega + \omega \rightarrow \phi \rightarrow (2 - u)\omega + u\omega$  via a resonance state  $\phi$ . (b) Symmetric-incident and coaxial scattering, where the incident angles of two photon wave vectors and their energies are symmetric, and the transverse momenta of photon pairs,  $p_T$ , always vanish with respect to the common optical axis  $z$ . (c) Asymmetric-incident and non-coaxial scattering, where the incident angles of two photon wave vectors and their energies are asymmetric, resulting in a finite value of  $p_T$  with respect to the common optical axis  $z$ . The zero- $p_T$  axis ( $z'$ -axis) is always configurable for arbitrary pairs of two incident wave vectors.

where a scalar-type field  $\phi$  with effective coupling  $g/M$  to two photons is assumed. In the case of the dilaton, the predicted parameter space has  $M = M_{\text{P}}$  and  $g = (1/2 \sim 5)/(3\pi)\alpha_{qed}$  [7] with  $\alpha_{qed} = 1/137$ , implying that experiments are required to be sensitive to the gravitationally weak coupling domain.

We have advocated that stimulated photon–photon scattering in a Quasi-Parallel collision System (QPS), illustrated in Fig.1a, can drastically enhance the interaction rate [8]. Capturing a resonance state in an  $s$ -channel photon–photon scattering within the uncertainty on  $E_{cms}$  is the first key element of the proposed method. The second key element is the enhancement of the interaction rate by the technique discussed in Appendix, which relies on the stimulated nature of the two-body

photon–photon scattering process, adding a coherently co-propagating field as the inducing field. Among several possible collision geometries [8–11], QPS is the optimum geometry for the low mass range, having the widest accessible mass range possible for a single collision geometry. For simplicity, we have initially considered QPS with a symmetric incident angle  $\vartheta$ , as shown in Fig.1a [8]. This can be realized by focusing a photon beam with a single photon energy  $\omega$ . In this case,  $E_{cms}$  is expressed as

$$E_{cms} = 2\omega \sin \vartheta. \quad (1.2)$$

This allows experiments to have two knobs to handle  $E_{cms}$ . The choice of combination between photon energies and incident angles depends on the trade-off between the beam and sensor technologies. In QPS, description of the interaction is non-trivial due to the inherently wave-like nature of photons [9]. As we show in detail in Appendix, the interaction rate is increased when electromagnetic waves are confined to a short time scale. If the waves are confined to a short duration, then an energy uncertainty  $\delta\omega$  must be introduced according to the uncertainty principle for the energy-time relation or, equivalently, as a result of the Fourier transform from the time domain to the frequency domain. In addition, around the focal spot, the momentum uncertainty is also maximized due to the spatial localization of a beam field again based on the uncertainty principle for the momentum-space relation. This implies that the incident angles of electromagnetic waves must also fluctuate strongly. These situations require us to depart from the simplest geometry (i.e., from assuming symmetric energies and symmetric incident angles) and use a fully asymmetric geometry in QPS, as illustrated in Fig.1c. The extended parametrization associated with the fully asymmetric case is non-trivial, and we will show this in Appendix. The main finding allowed by the extension to the fully asymmetric case is that the probability that non-coaxial collisions (Fig.1c) will occur dominates the probability of coaxial collisions (Fig.1b).

In the following sections, we first consider the concept of the stimulated pulsed-radar collider. We then evaluate the expected sensitivity based on the parametrization including the fully asymmetric collision cases in QPS. In order to reach the gravitationally coupling dilaton field, we discuss two technological requirements toward the future laboratory search for the dilaton field. Finally, our conclusion is given.

## 2. CONCEPT OF STIMULATED PULSED-RADAR COLLIDER

Toward the direct detection of the dilaton field of  $m \sim 10^{-7}$  eV, if we consider only a laser source with single-photon energy  $\sim 1$  eV, the incident angle must be maintained at  $\sim 10^{-7}$  radians and it is likely impossible to perform the search on the ground with a focal distance greater than  $10^7$  m, assuming a beam diameter of  $\sim 1$  m.

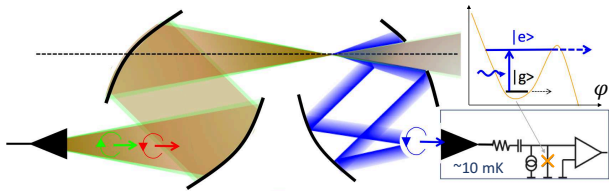


**FIG. 2:** Conceptual setup of the simulated radar collider and the detection of signal photons. Two circularly polarized coherent beams for creation (green, left-handed) and stimulation (red, right-handed) are combined and focused along a common optical axis. Signal photons (blue, right-handed) are emitted via the exchange of a dilaton field. Around the focal plane, only signal photons are partially reflected and collimated by a dichroic parabolic mirror with a hole through which intense GHz beams can escape the detection system, both to avoid adding thermal background sources and to avoid picking up atomic four-wave mixing processes from the upstream mirror surfaces as well as from residual gases in the focal spot, because these background photons are expected to be confined within the incident angles of the two beams. These peripherally emitted signal photons are focused into the detector element. The detector consists of a signal photon counter. For sensing GHz photons, for instance, a reasonable candidate is a Josephson-junction sensor based on a pulse-current-biased phase-qubit [12]. The bias instantaneously forms a potential, illustrated in the inset, as a function of the phase difference  $\varphi$  between two superconductors sandwiching an insulator gap. When a GHz-photon is absorbed in one of the two superconductors, the energy state of a Cooper pair transits from the ground state  $|g\rangle$  to an excited state  $|e\rangle$ , which drastically increases the probability for the Cooper pair to tunnel to the neighboring superconductor through the gap. This allows number-resolved counting if parallelized junctions are implemented [12].

However, if we could use an energy of  $\omega \sim 10^{-5}$  eV with incident angle  $\vartheta \sim 10^{-2}$  radians, it would be possible to focus the beam to within a few hundred meters for a beam having a diameter of a few meters and wavelength below 30 cm (1 GHz in frequency). Indeed, intense sources of GHz photons are already commercially available, such as the klystron [14]. Moreover, the number of photons per pulse is  $\sim 10^5$  times that of optical laser fields for the same pulse energy. Therefore, pulsed-radar beam in the GHz-band would be useful for a mass domain of  $\sim 10^{-7}$  eV. On the other hand, GHz photon counting with single-photon sensitivity is a difficult technological issue. In the area of GHz-photon sensing, some successful examples of single-photon detection with quantum-bit (qubit) technology have been reported recently [12, 13]. In particular, a phase-qubit sensor based on Josephson junctions [12] can be operated with a pulsed current bias within several ns duration [12]. This time-gated operation would reduce dark currents from continuous background blackbody radiation. Using the above considerations, Fig.2 illustrates a conceptual setup for a dilaton search in QPS with GHz-photon sources equipped with a

phase-qubit-type GHz-photon counter for the detection of signal photons.

Creation radar pulse	Klystron	Compress
central frequency $\nu_c$	2.8 GHz	
energy per pulse	100 J	
repetition rate $f$	50 Hz	
relative linewidth $\delta\nu_c/\nu_c \times 100$	$\pm 10^{-2}$ %	$\pm 5$ %
half pulse duration, $\tau_c$	1 $\mu$ s	0.568 ns
Inducing radar pulse	Klystron	Compress
central frequency $\nu_i$	1.6 GHz	
energy per pulse	100 J	
repetition rate $f$	50 Hz	
relative linewidth $\delta\nu_i/\nu_i \times 100$	$\pm 10^{-2}$ %	$\pm 5$ %
half pulse duration, $\tau_i$	1 $\mu$ s	0.995 ns
Measurement requirements	Klystron	Compress
central signal frequency $\nu_s$	4 GHz	
# of observed signals $N_{obs}$	100 photons	
data acquisition time $t_a$	1 month ( $2.6 \times 10^6$ )	
detector current bias time $\tau_b$	1 ns	
detector efficiency $\epsilon_d$	0.1	
overall efficiency $\epsilon \equiv \epsilon_d(\tau_b/2\tau_i)$	$5 \times 10^{-5}$	$5 \times 10^{-2}$
Geometric parameters in QPS		
creation beam diameter	6.02 m	
inducing beam diameter	6.10 m	
common focal length	30 m (five Rayleigh length)	

**TABLE I:** GHz-band pulsed beam parameters similar to the existing klystron [14] and the compressed case reaching the Fourier transform limit  $\tau_j \times 2\pi\delta\nu_j \geq 1/2$  for  $j = c$  or  $i$ .

### 3. EXPECTED SENSITIVITY

Given this stimulated radar collider setup with the experimental parameters set as listed in Tab.I, we discuss how we can reach the gravitational coupling domain in  $g/M < \alpha_{qed}/M_P$ , based on new formulas including an asymmetric quasi-parallel collision geometry, explained in Appendix in detail. In symmetric-incident and coaxial scattering in QPS (Fig.1b), transverse momenta of photon pairs,  $p_T$ , always vanish with respect to the common optical axis  $z$ . This guarantees that azimuthal angles of the final state photon wave vectors are axially symmetric around the  $z$ -axis. Therefore, the inducible momentum or angular range can be analytically obtained via the axial symmetric nature of the focused beams. On the other hand, in asymmetric-incident and non-coaxial scattering (Fig.1c), finite transverse momenta are unavoidably introduced. However, a zero- $p_T$  axis, defined as the  $z'$ -axis, is always configurable for any arbitrary pair of two incident wave vectors. Therefore,  $z'$ -axis can restore the axial symmetric nature of the azimuthal angles of the

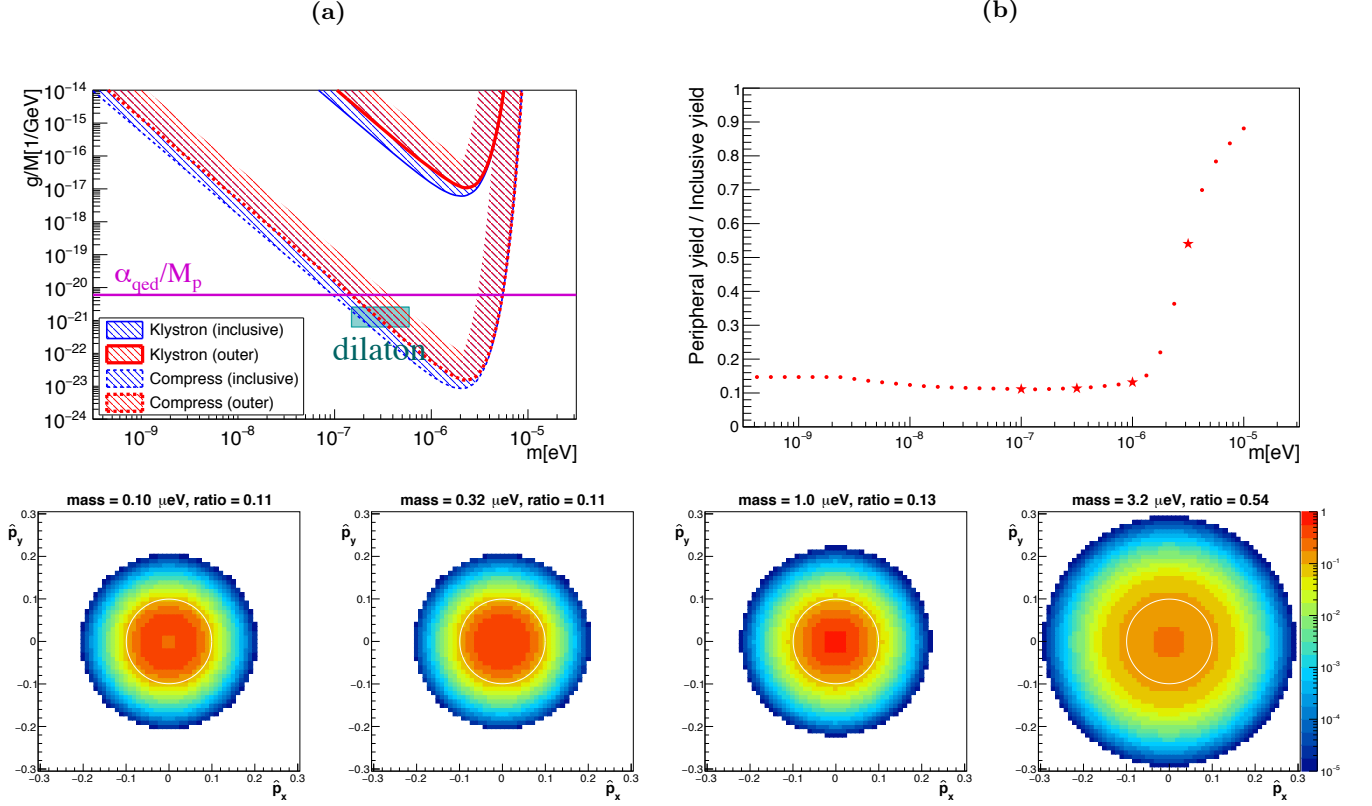


**FIG. 3:** Sensitivity curves and the ratio of outer emissions with the parameters listed in Tab.I. (a) Reachable coupling  $g/M$  vs. dilaton mass  $m$  domains. The shaded rectangular domain corresponds to the prediction from the dilaton model [7]. The domains above the solid curves show the reachable range with peak power and relative linewidth of GHz-photon pulses equivalent to an existing 100 MW klystron [14] (see the left column of Tab.I for the linewidth and pulse duration parameters). The dotted curves show the extended sensitivities when a relatively broader linewidth (the right column for the same parameters in Tab.I) is used; it is assumed a system capable of this will be developed in the near future. The thicker curves show the sensitivities when the signal photons are sampled only outside the divergence angles of the incident two beams. (b) The ratio of the signal photon yield emitted outside the divergence angles of incident beams to that of the inclusive yield as a function of mass. The lower four panels show the numerically calculated signal yields sampled at four mass points indicated with the star markers in the ratio plot as a function of the  $x$  and  $y$  components of unit momenta of signal photons,  $(\hat{p}_x, \hat{p}_y)$ , at the beam waist  $z = 0$ ; the white circles indicate the domains of beam divergence with the radius of  $\sin \Theta_0$  from Eq.(4.63) in Appendix. The color contours in the log scale are normalized to the common total number of signal photons.

final state wave vectors. Despite this, the inducing coherent field is physically mapped to the common optical axis  $z$ . Therefore, the inducible momentum range changes in a complicated manner that depends on an arbitrarily formed  $z'$ -axis. Hence, numerical integration must be performed to express the number of signal photons per shot  $\mathcal{Y}_{c+i}$  in Eq.(4.59) by substituting Eqs.(4.85) and (4.89), shown in Appendix. The number of experimentally observable signal photons  $N_{obs}$  as a function of mass and coupling for the set of experimental parameters  $P$  given in Tab.I is then expressed as

$$N_{obs} = \mathcal{Y}_{c+i}(m, g/M; P) t_a f \epsilon \quad (3.3)$$

where the data acquisition time is  $t_a$ , the repetition rate of pulsed beams is  $f$ , and the overall efficiency is  $\epsilon \equiv \epsilon_d(\tau_b/2\tau_i)$  with detection efficiency  $\epsilon_d$ , qubit current-bias time  $\tau_b$ , and inducing pulse duration  $\tau_i$ . By numerically solving this equation, we can obtain  $g/M$  for the given

values of  $m$  and  $N_{obs}$ . Dominant background photons are expected from blackbody radiations in the same spectrum width as that of the signal photons,  $(1 \pm \sim 0.05)\nu_s$ . The unavoidable blackbody source is the entrance horn connected to the qubit sensor. The total number of background photons is evaluated as  $N_{bkg} = 0.5$  photons by assuming that the horn and sensor temperatures are kept at  $T = 10$  mK with the inner surface area of the cone-type horn  $\Delta S = \pi \lambda_s^2$  for signal photon wavelength  $\lambda_s = c/\nu_s$  and solid angle  $\Delta \Omega = 2\pi$  from the following relation

$$N_{bkg} = \int_{0.95\nu_s}^{1.05\nu_s} \frac{2h\nu^3}{c^2} \frac{1}{e^{h\nu/(kT)} - 1} d\nu \frac{\Delta \Omega \Delta S t_a f \epsilon}{h\nu_s}. \quad (3.4)$$

We also note that photon-photon scattering in the SM can be neglected because the QED-based stimulated scattering is sufficiently suppressed by the  $E_{cms}^6$  dependence of the cross section [11, 15]. Considering systematic backgrounds, we require  $N_{obs} = 100 \gg N_{bkg}$  in this paper.

Figure 3a summarizes the accessible domains for coupling  $g/M$  versus mass  $m$ . This indicates that broadening the linewidth is indeed a key factor because it can increase the interaction rate by increasing the spacetime overlapping factor of the incident pulsed beams, as explained in Eq.(4.89), due to the short durations  $\tau_c$  and  $\tau_i$ , and also increases the chance to stimulate emission of final state photons satisfying energy-momentum conservation within the allowed energy-momentum fluctuations of collision beams, as indicated in Eq.(4.85) in Appendix. Figure 3b shows the ratio of signal photons found outside the angular divergence of the focused beams based on the geometric optics as a function of mass. For larger masses, larger fractions of signal photons are emitted to the outer angles. The non-coaxial collisions allow signal photon emission outside the divergence angles of the focused beams defined by geometric optics. Thanks to this scattering behavior, we can expect that the ratio between the number of signal photons and beam photons could be improved if we could measure only peripheral emissions

around the common optical axes, as illustrated in Fig.2.

#### 4. CONCLUSION

We have formulated stimulated resonant photon-photon scattering in QPS including asymmetric-incident and non-coaxial collisions. From the stimulated pulsed-radar collider concept, we expect that the sensitivity can reach the domain in which the dilaton field (a candidate for dark energy) is predicted to exist, assuming two key technological issues are resolved: pulse compression in time reaching the Fourier transform limit, and single-photon counting for GHz-band photons. These are possible in principle but technologically challenging in practice. It is worth being striving for them, however, because they would allow direct probing of gravitationally weak scattering processes in laboratory experiments, which has not been done in the history of science.

#### Acknowledgments

We express deep gratitude to Yasunori Fujii, who passed away in July 2019. This study is motivated by his outstanding works on the dilaton model and the effort to evaluate the concrete mass of a dilaton as well as coupling. We also thank K. Ishikawa for discussions about evaluation of the inducing effect, S. Mima and S. Shibata for discussions on the qubit application, and M. Oxborrow for discussions on pulsed GHz sources. K. Homma acknowledges the support of the Collaborative Research Program of the Institute for Chemical Research, Kyoto University (Grants Nos. 2018-83 and 2019-72) and Grants-in-Aid for Scientific Research Nos. 17H02897, 18H04354, and 19K21880 from the Ministry of Education, Culture, Sports, Science and Technology (MEXT) of Japan.

- 
- [1] M. Tanabashi et al. (Particle Data Group), Phys. Rev. D 98, 030001 (2018).
  - [2] Y. Nambu, Phys. Rev. Lett. 4, 380 (1960); J. Goldstone, Nuovo Cimento 19, 154 (1961).
  - [3] Y. Fujii, Nature Physical Science 234, 5-7 (1971).
  - [4] E. Fischbach and C. Talmadge, Nature 356, 207 (1992).
  - [5] Y. Fujii and K. Maeda, *The Scalar-Tensor Theory of Gravitation* (Cambridge University Press, 2003).
  - [6] P. Jordan, *Schwerkraft und Weltall* (Friedrich Vieweg und Sohn, Brunschweig, 1955).
  - [7] Y. Fujii, Fundam. Theor. Phys. 183 (2016) 59-75
  - [8] Y. Fujii and K. Homma, Prog. Theor. Phys **126**, 531 (2011); Prog. Theor. Exp. Phys. 089203 (2014) [erratum].
  - [9] K. Homma, T. Hasebe, and K.Kume, Prog. Theor. Exp. Phys. 083C01 (2014).
  - [10] T. Hasebe, K. Homma, Y. Nakamiya, K. Matsuura, K. Otani, M. Hashida, S. Inoue, S. Sakabe, Prog. Theor. Exp. Phys. 073C01 (2015).
  - [11] K. Homma and Y. Toyota, Prog. Theor. Exp. Phys. 2017, 063C01 (2017).
  - [12] Y.-F. Chen et al., Phys. Rev. Lett. 107, 217401 (2011).
  - [13] K. Inomata, Nature Communications 7, 12303 (2016).
  - [14] Pulsed klystron E3712.  
<https://etd.canon/ja/product/category/microwave/klystron.html>
  - [15] K. Homma, K. Matsuura, and K. Nakajima, Prog. Theor. Exp. Phys. 083C01 (2014).
  - [16] C. Möller, *General Properties of the Characteristic Matrix in the Theory of Elementary Particles*. I Munksgaard 1st edition (1946).
  - [17] M. A. Furman, LBNL-53553, CBP Note-543.
  - [18] J. D. Bjorken and S. D. Drell, *Relativistic Quantum Mechanics*, McGraw-Hill, Inc. (1964); See also Eq.(3.80) in W. Greiner and J. Reinhardt, *Quantum Electrodynamics Second Edition*, Springer (1994).
  - [19] R. J. Glauber, Phys. Rev. **131** (1963), 2766.
  - [20] Amnon Yariv, *Optical Electronics in Modern Communications* (Oxford University Press, 1997).

## Appendix

Here, we provide full details of the evaluation of signal yield in stimulated resonant photon–photon scattering in a quasi-parallel collision system (QPS) that includes fully asymmetric collision and stimulation geometries due to uncertainties regarding energy and incident angles in QPS. Figure 3 is calculated from numerical integration of Eq.(4.59) with Eqs.(4.85) and (4.89), using the parameter values given in Tab.I. We use the metric convention (+ – – –) throughout this appendix.

### A. Lorentz-invariant transition amplitude in the sea of coherent fields

The S-matrix for the interaction Lagrangian

$$- \mathcal{L} = gM^{-1} \frac{1}{4} F_{\mu\nu} F^{\mu\nu} \phi \quad (4.5)$$

is expressed as

$$S^{(2)} = \left( -\frac{1}{4} \frac{g}{M} \right)^2 \frac{i^2}{2} \int d^4x \int d^4y \quad (4.6)$$

$$\times T[F_{\mu\nu}(x) F^{\mu\nu} \phi(x) F_{\rho\sigma}(y) F^{\rho\sigma}(y) \phi(y)],$$

where  $T$  denotes the time-ordered product. From Wick's theorem, the T-product can be converted to the normal-ordering product by requiring contractions with four external electromagnetic fields, as follows.

$$N[F_{\mu\nu}(x) F^{\mu\nu}(x) F_{\sigma\rho}(y) F^{\sigma\rho}(y) \langle 0|T[\phi(x)\phi(y)]|0\rangle] \quad (4.7)$$

Here,

$$i \langle 0|T[\phi(x)\phi(y)]|0\rangle \equiv \frac{1}{(2\pi)^4} \int d^4q \frac{e^{-iq(x-y)}}{m^2 - q^2 - i\epsilon} \quad (4.8)$$

is the propagator of a massive scalar field  $\phi$  with an infinitesimal number  $\epsilon$ . We expand the field strength tensor as

$$F^{\mu\nu} \equiv (-i) \int \frac{d^3\mathbf{p}}{(2\pi)^3 2p^0} \Sigma_{\lambda=1,2} (P^{\mu\nu} e^{-ipx} a_{\mathbf{p},\lambda} + \hat{P}^{\mu\nu} e^{ipx} a_{\mathbf{p},\lambda}^\dagger) \quad (4.9)$$

and further define the following momentum-polarization tensors as capitalized symbols for an arbitrary four-momentum  $p$  of the electromagnetic field with the polarization state  $\lambda$ :

$$P^{\mu\nu} \equiv p^\mu \epsilon^\nu(p, \lambda) - \epsilon^\mu(p, \lambda) p^\nu, \quad (4.10)$$

$$\hat{P}^{\mu\nu} \equiv \epsilon^{*\mu}(p, \lambda) p^\nu - p^\mu \epsilon^{*\nu}(p, \lambda).$$

The commutation relations are

$$[a_{\mathbf{k},\lambda}, a_{\mathbf{k}',\lambda'}^\dagger] = (2\pi)^3 2p^0 \delta^3(\mathbf{k} - \mathbf{k}') \delta(\lambda - \lambda'), \quad (4.11)$$

$$[a_{\mathbf{k},\lambda}, a_{\mathbf{k}',\lambda'}] = [a_{\mathbf{k},\lambda}^\dagger, a_{\mathbf{k}',\lambda'}^\dagger] = 0.$$

From here, we omit the polarization index  $\lambda$  and the sum over it for the photon creation and annihilation operators,  $a_{\mathbf{p},\lambda}$  and  $a_{\mathbf{p},\lambda}^\dagger$ , because we require fixed beam polarizations in the last step of the following calculations. Substituting Eqs.(4.7–4.10) into (4.6), we get

$$S^{(2)} = \left( -\frac{1}{4} \frac{g}{M} \right)^2 \frac{i}{2} \int d^4x \int d^4y \int \frac{d^4q}{(2\pi)^4} \frac{e^{-iq(x-y)}}{m^2 - q^2 - i\epsilon} \times \quad (4.12)$$

$$(-i)^4 \int \frac{d^3\mathbf{s}}{(2\pi)^3 2s^0} \int \frac{d^3\mathbf{t}}{(2\pi)^3 2t^0} \int \frac{d^3\mathbf{u}}{(2\pi)^3 2u^0} \int \frac{d^3\mathbf{v}}{(2\pi)^3 2v^0} \times$$

$$T[ (S_{\mu\nu} T^{\mu\nu} e^{-i(s+t)x} a_{\mathbf{s}} a_{\mathbf{t}} + S_{\mu\nu} \hat{T}^{\mu\nu} e^{-i(s-t)x} a_{\mathbf{s}} a_{\mathbf{t}}^\dagger +$$

$$\hat{S}_{\rho\sigma} T^{\rho\sigma} e^{-i(t-s)x} a_{\mathbf{s}}^\dagger a_{\mathbf{t}} + \hat{S}_{\rho\sigma} \hat{T}^{\rho\sigma} e^{i(s+t)x} a_{\mathbf{s}}^\dagger a_{\mathbf{t}}^\dagger) \times$$

$$(U_{\mu\nu} V^{\mu\nu} e^{-i(u+v)y} a_{\mathbf{u}} a_{\mathbf{v}} + U_{\mu\nu} \hat{V}^{\mu\nu} e^{-i(u-v)y} a_{\mathbf{u}} a_{\mathbf{v}}^\dagger +$$

$$\hat{U}_{\rho\sigma} V^{\rho\sigma} e^{-i(v-u)y} a_{\mathbf{u}}^\dagger a_{\mathbf{v}} + \hat{U}_{\rho\sigma} \hat{V}^{\rho\sigma} e^{i(u+v)y} a_{\mathbf{u}}^\dagger a_{\mathbf{v}}^\dagger) ].$$

Since we focus on only two-body–two-body interactions, the relevant S-matrix (including two creation and two annihilation operators) is expressed as

$$S_{2 \rightarrow 2}^{(2)} = \left( -\frac{1}{4} \frac{g}{M} \right)^2 \frac{i}{2} (2\pi)^4 \times \quad (4.13)$$

$$\int \frac{d^3\mathbf{s}}{(2\pi)^3 2s^0} \int \frac{d^3\mathbf{t}}{(2\pi)^3 2t^0} \int \frac{d^3\mathbf{u}}{(2\pi)^3 2u^0} \int \frac{d^3\mathbf{v}}{(2\pi)^3 2v^0} \times$$

$$(G_{-s,-t} \delta^4(-u-v+s+t) S_{\mu\nu} T^{\mu\nu} \hat{U}_{\rho\sigma} \hat{V}^{\rho\sigma} a_{\mathbf{u}}^\dagger a_{\mathbf{v}}^\dagger a_{\mathbf{s}} a_{\mathbf{t}} +$$

$$G_{-s,+t} \delta^4(+u-v+s-t) S_{\mu\nu} \hat{T}^{\mu\nu} U_{\rho\sigma} \hat{V}^{\rho\sigma} a_{\mathbf{t}}^\dagger a_{\mathbf{v}}^\dagger a_{\mathbf{s}} a_{\mathbf{u}} +$$

$$G_{-s,+t} \delta^4(-u+v+s-t) S_{\mu\nu} \hat{T}^{\mu\nu} \hat{U}_{\rho\sigma} V^{\rho\sigma} a_{\mathbf{t}}^\dagger a_{\mathbf{u}}^\dagger a_{\mathbf{s}} a_{\mathbf{v}} +$$

$$G_{+s,-t} \delta^4(+u-v-s+t) \hat{S}_{\mu\nu} T^{\mu\nu} U_{\rho\sigma} \hat{V}^{\rho\sigma} a_{\mathbf{s}}^\dagger a_{\mathbf{v}}^\dagger a_{\mathbf{t}} a_{\mathbf{u}} +$$

$$G_{+s,-t} \delta^4(-u+v-s+t) \hat{S}_{\mu\nu} T^{\mu\nu} \hat{U}_{\rho\sigma} V^{\rho\sigma} a_{\mathbf{s}}^\dagger a_{\mathbf{u}}^\dagger a_{\mathbf{t}} a_{\mathbf{v}} +$$

$$G_{+s,+t} \delta^4(+u+v-s-t) \hat{S}_{\mu\nu} \hat{T}^{\mu\nu} U_{\rho\sigma} V^{\rho\sigma} a_{\mathbf{s}}^\dagger a_{\mathbf{t}}^\dagger a_{\mathbf{u}} a_{\mathbf{v}}),$$

where  $G_{i,j} \equiv (m^2 - (i+j)^2)^{-1}$  indicate corresponding propagators.

Let us recall the definition of the coherent state [19]:

$$|N_{\mathbf{p}}\rangle \equiv \exp(-N_{\mathbf{p}}/2) \sum_{n=0}^{\infty} \frac{N_{\mathbf{p}}^{n/2}}{\sqrt{n!}} |n_{\mathbf{p}}\rangle, \quad (4.14)$$

where  $|n_{\mathbf{p}}\rangle$  is the normalized state of  $n$  photons

$$|n_{\mathbf{p}}\rangle = \frac{1}{\sqrt{n!}} (a_{\mathbf{p}}^\dagger)^n |0\rangle, \quad (4.15)$$

with the creation operator  $a_{\mathbf{p}}^\dagger$  of photons that share a common momentum  $\mathbf{p}$  and a common polarization state over different number states. The following relations on the coherent state

$$\langle\langle N_{\mathbf{p}} | N_{\mathbf{p}} \rangle\rangle = 1 \quad (4.16)$$

and

$$\langle\langle N_{\mathbf{p}} | n | N_{\mathbf{p}} \rangle\rangle = \langle\langle N_{\mathbf{p}} | (a_{\mathbf{p}}^\dagger a_{\mathbf{p}}) | N_{\mathbf{p}} \rangle\rangle = N_{\mathbf{p}}, \quad (4.17)$$

give us basic properties with respect to the creation and annihilation operators:

$$a_{\mathbf{p}}|N_{\mathbf{p}}\rangle\rangle = \sqrt{N_{\mathbf{p}}}|N_{\mathbf{p}}\rangle\rangle, \quad \text{and} \quad \langle\langle N_{\mathbf{p}}|a_{\mathbf{p}}^\dagger = \sqrt{N_{\mathbf{p}}}\langle\langle N_{\mathbf{p}}|. \quad (4.18)$$

We first consider a search for signal photons  $p_3$  via the scattering process  $p_1 + p_2 \rightarrow p_3 + p_4$  by supplying coherent fields  $|N_{\mathbf{p}_1}\rangle\rangle$ ,  $|N_{\mathbf{p}_2}\rangle\rangle$  and  $|N_{\mathbf{p}_4}\rangle\rangle$ . We then introduce initial and final states, respectively, as follows:

$$|\Omega\rangle \equiv |N_{\mathbf{p}_1}\rangle\rangle|N_{\mathbf{p}_2}\rangle\rangle|N_{\mathbf{p}_4}\rangle\rangle|0\rangle, \quad \text{and} \quad (4.19)$$

$$\langle\Omega'| \equiv \langle\langle N_{\mathbf{p}_1}|\langle\langle N_{\mathbf{p}_2}|\langle\langle N_{\mathbf{p}_4}|\langle 1_{\mathbf{p}_3}| = \langle\Omega|a_{\mathbf{p}_3}.$$

The two-body transition amplitude  $\langle\Omega'|S_{2\rightarrow 2}^{(2)}|\Omega\rangle$  contains the common operator products  $a_i^\dagger a_j^\dagger a_{\mathbf{k}} a_{\mathbf{l}}$ . We then separately evaluate the contractions with coherent bra- and ket-states, respectively, as follows:

$$\begin{aligned} \langle\Omega'|a_i^\dagger a_j^\dagger &= \sqrt{N_{p_1}}\hat{\delta}^3(\mathbf{p}_1 - \mathbf{i}) \times & (4.20) \\ &\{\langle\Omega'|\sqrt{N_{p_1}}\hat{\delta}^3(\mathbf{p}_1 - \mathbf{j}) + \langle\Omega'|\sqrt{N_{p_2}}\hat{\delta}^3(\mathbf{p}_2 - \mathbf{j}) + \\ &\langle\Omega'|\sqrt{N_{p_4}}\hat{\delta}^3(\mathbf{p}_4 - \mathbf{j}) + \langle\Omega|1\hat{\delta}^3(\mathbf{p}_3 - \mathbf{j})\} + \\ &\quad \sqrt{N_{p_2}}\hat{\delta}^3(\mathbf{p}_2 - \mathbf{i}) \times \\ &\{\langle\Omega'|\sqrt{N_{p_1}}\hat{\delta}^3(\mathbf{p}_1 - \mathbf{j}) + \langle\Omega'|\sqrt{N_{p_2}}\hat{\delta}^3(\mathbf{p}_2 - \mathbf{j}) + \\ &\langle\Omega'|\sqrt{N_{p_4}}\hat{\delta}^3(\mathbf{p}_4 - \mathbf{j}) + \langle\Omega|1\hat{\delta}^3(\mathbf{p}_3 - \mathbf{j})\} + \\ &\quad \sqrt{N_{p_4}}\hat{\delta}^3(\mathbf{p}_4 - \mathbf{i}) \times \\ &\{\langle\Omega'|\sqrt{N_{p_1}}\hat{\delta}^3(\mathbf{p}_1 - \mathbf{j}) + \langle\Omega'|\sqrt{N_{p_2}}\hat{\delta}^3(\mathbf{p}_2 - \mathbf{j}) + \\ &\langle\Omega'|\sqrt{N_{p_4}}\hat{\delta}^3(\mathbf{p}_4 - \mathbf{j}) + \langle\Omega|1\hat{\delta}^3(\mathbf{p}_3 - \mathbf{j})\} + \\ &\quad 1\hat{\delta}^3(\mathbf{p}_3 - \mathbf{i}) \times \\ &\{\langle\Omega|\sqrt{N_{p_1}}\hat{\delta}^3(\mathbf{p}_1 - \mathbf{j}) + \langle\Omega|\sqrt{N_{p_2}}\hat{\delta}^3(\mathbf{p}_2 - \mathbf{j}) + \\ &\langle\Omega|\sqrt{N_{p_4}}\hat{\delta}^3(\mathbf{p}_4 - \mathbf{j}) + \langle\Omega|a_j^\dagger\}, \end{aligned}$$

where the last term vanishes because  $\langle 0|a_{\mathbf{p}}^\dagger = 0$ , and

$$\begin{aligned} a_{\mathbf{k}} a_{\mathbf{l}} |\Omega\rangle &= \sqrt{N_{p_1}}\hat{\delta}^3(\mathbf{p}_1 - \mathbf{l})\{\sqrt{N_{p_1}}\hat{\delta}^3(\mathbf{p}_1 - \mathbf{k})|\Omega\rangle + & (4.21) \\ &\sqrt{N_{p_2}}\hat{\delta}^3(\mathbf{p}_2 - \mathbf{k})|\Omega\rangle + \sqrt{N_{p_4}}\hat{\delta}^3(\mathbf{p}_4 - \mathbf{k})|\Omega\rangle\} + \\ &\sqrt{N_{p_2}}\hat{\delta}^3(\mathbf{p}_2 - \mathbf{l})\{\sqrt{N_{p_1}}\hat{\delta}^3(\mathbf{p}_1 - \mathbf{k})|\Omega\rangle + \\ &\sqrt{N_{p_2}}\hat{\delta}^3(\mathbf{p}_2 - \mathbf{k})|\Omega\rangle + \sqrt{N_{p_4}}\hat{\delta}^3(\mathbf{p}_4 - \mathbf{k})|\Omega\rangle\} + \\ &\sqrt{N_{p_4}}\hat{\delta}^3(\mathbf{p}_4 - \mathbf{l})\{\sqrt{N_{p_1}}\hat{\delta}^3(\mathbf{p}_1 - \mathbf{k})|\Omega\rangle + \\ &\sqrt{N_{p_2}}\hat{\delta}^3(\mathbf{p}_2 - \mathbf{k})|\Omega\rangle + \sqrt{N_{p_4}}\hat{\delta}^3(\mathbf{p}_4 - \mathbf{k})|\Omega\rangle\}. \end{aligned}$$

Because the search window is designed for the scattering process  $p_1 + p_2 \rightarrow p_3 + p_4$ , the consistent transition amplitude that satisfies the combination of the initial and final state momenta is limited to

$$\begin{aligned} \langle\Omega'|a_i^\dagger a_j^\dagger a_{\mathbf{k}} a_{\mathbf{l}}|\Omega\rangle &= \{\sqrt{N_{p_4}}\hat{\delta}^3(\mathbf{p}_4 - \mathbf{i})1\hat{\delta}^3(\mathbf{p}_3 - \mathbf{j}) + 1\hat{\delta}^3(\mathbf{p}_3 - \mathbf{i})\sqrt{N_{p_4}}\hat{\delta}^3(\mathbf{p}_4 - \mathbf{j})\} \times & (4.22) \\ &\{\sqrt{N_{p_1}}\hat{\delta}^3(\mathbf{p}_1 - \mathbf{l})\sqrt{N_{p_2}}\hat{\delta}^3(\mathbf{p}_2 - \mathbf{k}) + \sqrt{N_{p_2}}\hat{\delta}^3(\mathbf{p}_2 - \mathbf{l})\sqrt{N_{p_1}}\hat{\delta}^3(\mathbf{p}_1 - \mathbf{k})\}\langle\Omega|\Omega\rangle \\ &= \sqrt{N_{p_1}}\sqrt{N_{p_2}}\sqrt{N_{p_4}}\{\hat{\delta}^3(\mathbf{p}_4 - \mathbf{i})\hat{\delta}^3(\mathbf{p}_3 - \mathbf{j})\hat{\delta}^3(\mathbf{p}_2 - \mathbf{k})\hat{\delta}^3(\mathbf{p}_1 - \mathbf{l}) + \\ &\quad \hat{\delta}^3(\mathbf{p}_4 - \mathbf{i})\hat{\delta}^3(\mathbf{p}_3 - \mathbf{j})\hat{\delta}^3(\mathbf{p}_1 - \mathbf{k})\hat{\delta}^3(\mathbf{p}_2 - \mathbf{l}) + \\ &\quad \hat{\delta}^3(\mathbf{p}_3 - \mathbf{i})\hat{\delta}^3(\mathbf{p}_4 - \mathbf{j})\hat{\delta}^3(\mathbf{p}_2 - \mathbf{k})\hat{\delta}^3(\mathbf{p}_1 - \mathbf{l}) + \\ &\quad \hat{\delta}^3(\mathbf{p}_3 - \mathbf{i})\hat{\delta}^3(\mathbf{p}_4 - \mathbf{j})\hat{\delta}^3(\mathbf{p}_1 - \mathbf{k})\hat{\delta}^3(\mathbf{p}_2 - \mathbf{l})\}, \end{aligned}$$

where  $\langle\Omega|\Omega\rangle = 1$  is used.

By assigning any of  $\mathbf{i}, \mathbf{j}, \mathbf{k}$ , and  $\mathbf{l}$  in Eq.(4.22) to any of

$\mathbf{s}, \mathbf{t}, \mathbf{u}, \mathbf{v}$  in Eq.(4.13), the two-body transition amplitude can be expressed as

$$\langle \Omega' | S_{2 \rightarrow 2}^{(2)} | \Omega \rangle = \left( -\frac{1}{4} \frac{g}{M} \right)^2 \frac{i}{2} (2\pi)^4 \delta^{(4)}(p_1 + p_2 - p_3 - p_4) \sqrt{N_{p_1}} \sqrt{N_{p_2}} \sqrt{N_{p_4}} \times \quad (4.23)$$

$$\left( \frac{8(P_1 P_2)(\hat{P}_3 \hat{P}_4)}{m^2 - (p_1 + p_2)^2} + \frac{4(P_2 \hat{P}_4)(P_1 \hat{P}_3)}{m^2 - (p_2 - p_4)^2} + \frac{4(P_2 \hat{P}_3)(P_1 \hat{P}_4)}{m^2 - (p_2 - p_3)^2} + \frac{4(P_1 \hat{P}_4)(P_2 \hat{P}_3)}{m^2 - (p_1 - p_4)^2} + \frac{4(P_1 \hat{P}_3)(P_2 \hat{P}_4)}{m^2 - (p_1 - p_3)^2} \right),$$

where subscripts have been omitted in the momentum-polarization tensors such as  $(S\hat{T}) \equiv S_{\mu\nu} \hat{T}^{\mu\nu}$ .

From the experimental point of view, it is also useful to consider the case  $p_1 + p_1 \rightarrow p_3 + p_4$ , where the initial state photons are from a degenerate state, because the number of incident beams can be reduced from two to one in an experimental setup. For the degenerate case, we define the initial and final states, respectively, as follows:

$$|\Omega\rangle \equiv |N_{p_1}\rangle |N_{p_4}\rangle |0\rangle, \text{ and} \quad (4.24)$$

$$\langle \Omega' | \equiv \langle \langle N_{p_1} | \langle \langle N_{p_4} | \langle \langle 1_{p_3} | = \langle \Omega | a_{p_3}.$$

For the evaluation of the two-body transition amplitude  $\langle \Omega' | S_{2 \rightarrow 2}^{(2)} | \Omega \rangle$  containing  $a_i^\dagger a_j^\dagger a_k a_l$ , we again separately evaluate the contractions with coherent bra- and ket-states, respectively, as follows:

$$\langle \Omega' | a_i^\dagger a_j^\dagger = \sqrt{N_{p_1}} \delta^3(\mathbf{p}_1 - \mathbf{i}) \times \quad (4.25)$$

$$\{ \langle \Omega' | \sqrt{N_{p_1}} \delta^3(\mathbf{p}_1 - \mathbf{j}) + \langle \Omega' | \sqrt{N_{p_4}} \delta^3(\mathbf{p}_4 - \mathbf{j}) + \langle \Omega | 1 \delta^3(\mathbf{p}_3 - \mathbf{j}) \} +$$

$$\sqrt{N_{p_4}} \delta^3(\mathbf{p}_4 - \mathbf{i}) \times$$

$$\{ \langle \Omega' | \sqrt{N_{p_1}} \delta^3(\mathbf{p}_1 - \mathbf{j}) + \langle \Omega' | \sqrt{N_{p_4}} \delta^3(\mathbf{p}_4 - \mathbf{j}) + \langle \Omega | 1 \delta^3(\mathbf{p}_3 - \mathbf{j}) \} +$$

$$1 \delta^3(\mathbf{p}_3 - \mathbf{i}) \times$$

$$\{ \langle \Omega | \sqrt{N_{p_1}} \delta^3(\mathbf{p}_1 - \mathbf{j}) + \langle \Omega | \sqrt{N_{p_4}} \delta^3(\mathbf{p}_4 - \mathbf{j}) + \langle \Omega | a_j^\dagger \},$$

where the last term vanishes because  $\langle 0 | a_{\mathbf{p}}^\dagger = 0$ , and

$$a_k a_l | \Omega \rangle = \sqrt{N_{p_1}} \delta^3(\mathbf{p}_1 - \mathbf{l}) \times \quad (4.26)$$

$$\{ \sqrt{N_{p_1}} \delta^3(\mathbf{p}_1 - \mathbf{k}) | \Omega \rangle + \sqrt{N_{p_4}} \delta^3(\mathbf{p}_4 - \mathbf{k}) | \Omega \rangle \} +$$

$$\sqrt{N_{p_4}} \delta^3(\mathbf{p}_4 - \mathbf{l}) \times$$

$$\{ \sqrt{N_{p_1}} \delta^3(\mathbf{p}_1 - \mathbf{k}) | \Omega \rangle + \sqrt{N_{p_4}} \delta^3(\mathbf{p}_4 - \mathbf{k}) | \Omega \rangle \}.$$

The consistent transition amplitude that satisfies the combination of the initial and final state momenta in the degenerate case is expressed as

$$\langle \Omega' | a_i^\dagger a_j^\dagger a_k a_l | \Omega \rangle = \{ \sqrt{N_{p_4}} \delta^3(\mathbf{p}_4 - \mathbf{i}) 1 \delta^3(\mathbf{p}_3 - \mathbf{j}) + \quad (4.27)$$

$$1 \delta^3(\mathbf{p}_3 - \mathbf{i}) \sqrt{N_{p_4}} \delta^3(\mathbf{p}_4 - \mathbf{j}) \} \times$$

$$\sqrt{N_{p_1}} \delta^3(\mathbf{p}_1 - \mathbf{l}) \sqrt{N_{p_1}} \delta^3(\mathbf{p}_1 - \mathbf{k}) \langle \Omega | \Omega \rangle$$

$$= \sqrt{N_{p_1}} \sqrt{N_{p_1}} \sqrt{N_{p_4}} \times$$

$$\{ \delta^3(\mathbf{p}_4 - \mathbf{i}) \delta^3(\mathbf{p}_3 - \mathbf{j}) \delta^3(\mathbf{p}_1 - \mathbf{k}) \delta^3(\mathbf{p}_1 - \mathbf{l}) +$$

$$\delta^3(\mathbf{p}_3 - \mathbf{i}) \delta^3(\mathbf{p}_4 - \mathbf{j}) \delta^3(\mathbf{p}_1 - \mathbf{k}) \delta^3(\mathbf{p}_1 - \mathbf{l}) \},$$

where  $\langle \Omega | \Omega \rangle = 1$  is substituted.

Again assigning any of  $\mathbf{i}, \mathbf{j}, \mathbf{k}$ , and  $\mathbf{l}$  in Eq.(4.27) to any of  $\mathbf{s}, \mathbf{t}, \mathbf{u}$ , and  $\mathbf{v}$  in Eq.(4.13), the two-body transition amplitude is expressed as

$$\langle \Omega' | S_{2 \rightarrow 2}^{(2)} | \Omega \rangle = \left( -\frac{1}{4} \frac{g}{M} \right)^2 \frac{i}{2} (2\pi)^4 \delta^{(4)}(p_1 + p_1 - p_3 - p_4) \sqrt{N_{p_1}} \sqrt{N_{p_1}} \sqrt{N_{p_4}} \times \quad (4.28)$$

$$\left( \frac{4(P_1 P_1)(\hat{P}_3 \hat{P}_4)}{m^2 - (p_1 + p_1)^2} + \frac{4(P_1 \hat{P}_4)(P_1 \hat{P}_3)}{m^2 - (p_1 - p_4)^2} + \frac{4(P_1 \hat{P}_3)(P_1 \hat{P}_4)}{m^2 - (p_1 - p_3)^2} \right).$$

We take special note that the degenerate case may also be interpreted as a special case of the non-degenerate case by reducing the average number of  $p_1$  photons from  $N_{p_1}$  to  $N_{p_1}/2$  due to the equal split into two identical beams and equating 1 and 2 in the subscripts in Eq.(4.23).

## B. Kinematics in asymmetric-incident and non-coaxial geometry in QPS

As illustrated in Fig.4, we extend the scattering formulation to the most general scattering geometry, which is asymmetric-incident and non-coaxial scattering in QPS.

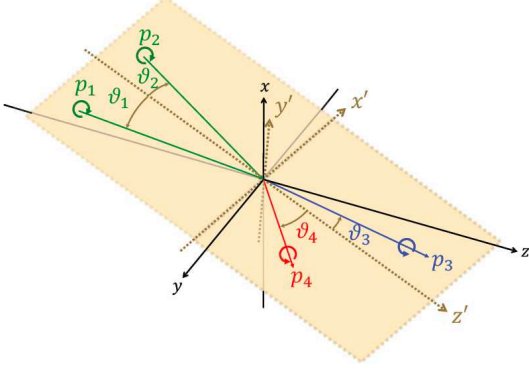


**FIG. 4:** Kinematical parameters in asymmetric-incident and non-coaxial geometry. Primed coordinates  $(x', y', z')$ , where the total transverse momentum of an arbitrary selected pair of incident photons within the creation beam vanishes, are configurable with respect to the fixed laboratory coordinate  $(x, y, z)$  to which the focused beam fields are physically mapped. The kinematical parameters used to derive the scattering amplitude are all based on these primed coordinates.

For a selected pair of incident waves,  $p_1$  and  $p_2$ , from a coherent creation beam, we can always define an axis  $z'$  around which the total transverse momentum,  $p_T$ , of the two incident waves becomes zero and an axis  $x'$  normal to the  $z'$ -axis on the reaction plane that includes the two wave vectors, as shown in Fig.4. On this  $x' - z'$  plane, referred to as the *zero- $p_T$  coordinate*, the scattering amplitude is greatly simplified because the emission angles of final state waves  $p_3$  and  $p_4$  become axially symmetric around the  $z'$ -axis. The labels for energies are common to both the zero- $p_T$  coordinate and the laboratory coordinate defined in terms of the  $x, y$ , and  $z$ -axes, while angular or momentum labels are valid only for the zero- $p_T$  coordinate. In the following subsections, for simplicity, we use kinematical parameters defined in the zero- $p_T$  coordinate, even when the prime symbol is not written, except where laboratory coordinates are explicitly specified.

With the energies of four photons  $\omega_i$  and scattering angles  $\vartheta_i$  for initial  $i = 1, 2$  and final  $i = 3, 4$  states in the zero- $p_T$  coordinate, four-momenta are defined as follows:

$$\begin{aligned} p_1 &= (\omega_1, \omega_1 \sin \vartheta_1, 0, \omega_1 \cos \vartheta_1), \\ p_2 &= (\omega_2, -\omega_2 \sin \vartheta_2, 0, \omega_2 \cos \vartheta_2), \\ p_3 &= (\omega_3, \omega_3 \sin \vartheta_3, 0, \omega_3 \cos \vartheta_3), \\ p_4 &= (\omega_4, -\omega_4 \sin \vartheta_4, 0, \omega_4 \cos \vartheta_4). \end{aligned} \quad (4.29)$$

For later convenience, a bisecting angle  $\vartheta_b$  is introduced, with the meaning

$$\vartheta_b \equiv \frac{\vartheta_1 + \vartheta_2}{2}. \quad (4.30)$$

The energy-momentum conservation equalities are

$$\begin{aligned} \omega_1 + \omega_2 &= \omega_3 + \omega_4 & (4.31) \\ \omega_1 \cos \vartheta_1 + \omega_2 \cos \vartheta_2 &= \omega_3 \cos \vartheta_3 + \omega_4 \cos \vartheta_4 \equiv \omega_z \\ \omega_1 \sin \vartheta_1 - \omega_2 \sin \vartheta_2 &= \omega_3 \sin \vartheta_3 - \omega_4 \sin \vartheta_4 \equiv \omega_x \end{aligned}$$

The corresponding center-of-mass energy,  $E_{c.m.s}$ , is then expressed as

$$E_{c.m.s} = \sqrt{2\omega_1\omega_2\{1 - \cos(\vartheta_1 + \vartheta_2)\}} = 2\sqrt{\omega_1\omega_2} \sin \vartheta_b. \quad (4.32)$$

We then define the linear polarization vectors as

$$\begin{aligned} e_i^{(1)} &= (0, 1, 0), & (4.33) \\ e_1^{(2)} &= (-\cos \vartheta_1, 0, \sin \vartheta_1), \\ e_2^{(2)} &= (-\cos \vartheta_2, 0, -\sin \vartheta_2), \\ e_3^{(2)} &= (-\cos \vartheta_3, 0, \sin \vartheta_3), \\ e_4^{(2)} &= (-\cos \vartheta_4, 0, -\sin \vartheta_4). \end{aligned}$$

With the linear polarization vectors, we also can define circular polarization states:

$$\begin{aligned} e_i^R &= \frac{1}{\sqrt{2}}(e_i^{(1)} + ie_i^{(2)}), & (4.34) \\ e_i^L &= \frac{1}{\sqrt{2}}(e_i^{(1)} - ie_i^{(2)}). \end{aligned}$$

Given these definitions, we can evaluate the momentum-polarization tensors included in Eq.(4.23) for the circular polarization case as follows

$$\begin{aligned} (P_i P_j) &= (\hat{P}_i \hat{P}_j) = 2\omega_i \omega_j (1 - \cos(\vartheta_i + \vartheta_j)) & (4.35) \\ (P_i \hat{P}_j) &= (\hat{P}_i P_j) = 0. \end{aligned}$$

### C. Lorentz-invariant scattering amplitude including a resonance state

Here we are particularly interested in formulating a Lorentz-invariant scattering amplitude for circular polarization states, because the states describe naturally interpretable angular momenta of photons with respect to any directions of the photon momenta. We denote a sequence of four-photon circular polarization states as a subscript  $S \equiv abcd$  with  $a, b, c, d = R$  (right-handed) or  $L$  (left-handed). From the following definition for the transition amplitude

$$\begin{aligned} \langle \Omega' | S_{2 \rightarrow 2}^{(2)} | \Omega \rangle &= \sqrt{N_{p_1}} \sqrt{N_{p_2}} \sqrt{N_{p_4}} \times & (4.36) \\ & i(2\pi)^4 \delta^{(4)}(p_1 + p_2 - p_3 - p_4) \mathcal{M}_S, \end{aligned}$$

the Lorentz-invariant scattering amplitude  $\mathcal{M}_S$  can be expressed as

$$\mathcal{M}_S = \frac{1}{4} \left( \frac{g}{M} \right)^2 \frac{(P_1 P_2)(\hat{P}_3 \hat{P}_4)}{m^2 - (p_1 + p_2)^2} \quad (4.37)$$

from Eq.(4.23) by taking Eq.(4.35) into account, where we exclude the beam-relevant factor in the definition of  $\mathcal{M}_S$  so as to decouple the dynamics from the experimental factor caused by the coherent beam intensity. With Eq.(4.35), the vertex factors in the numerator of  $\mathcal{M}_S$  are expressed as

$$\begin{aligned} (P_1 P_2) &= 2\omega_1 \omega_2 (1 - \cos(\vartheta_1 + \vartheta_2)) \\ (\hat{P}_3 \hat{P}_4) &= 2\omega_3 \omega_4 (1 - \cos(\vartheta_3 + \vartheta_4)). \end{aligned} \quad (4.38)$$

Since energy-momentum conservation requires  $(p_1 + p_2)^2 = (p_3 + p_4)^2$ , we can describe the amplitude applicable to both  $S = LLRR$  and  $RRLL$  in terms of only the initial state variables, as follows:

$$\begin{aligned} \mathcal{M}_S &= \left(\frac{g}{M}\right)^2 \frac{(\omega_1 \omega_2 (\cos(\vartheta_1 + \vartheta_2) - 1))^2}{m^2 - 2\omega_1 \omega_2 (1 - \cos(\vartheta_1 + \vartheta_2))} \\ &= \left(\frac{g}{M}\right)^2 \frac{(2\omega_1 \omega_2 \sin^2 \vartheta_b)^2}{m^2 - 4\omega_1 \omega_2 \sin^2 \vartheta_b}, \end{aligned} \quad (4.39)$$

where Eq.(4.30) is substituted for the second relation. To implement energy fluctuations in the initial state of two photons chosen from a solo coherent beam around its central energy  $\omega_c$ , we introduce two independent parameters  $s_1$  and  $s_2$ , as follows:

$$\omega_1 = s_1 \omega_c, \quad \omega_2 = s_2 \omega_c. \quad (4.40)$$

We then define a resonance energy  $\omega_r$  satisfying  $E_{cms} = m$  as

$$\omega_r^2 \equiv \frac{m^2}{4s_1 s_2 \sin^2 \vartheta_b}. \quad (4.41)$$

Because the exchanged scalar field is (in principle) an unstable particle, we introduce a decay rate  $\Gamma$ , which is defined as [8]

$$\Gamma = \frac{1}{16\pi} \left(\frac{g}{M}\right)^2 m^3. \quad (4.42)$$

This causes a change in the mass square as  $m^2 \rightarrow (m - i\Gamma/2)^2 \approx m^2 - im\Gamma$ . Therefore, the denominator  $\mathcal{D}$  in Eq.(4.39) is expressed as

$$\begin{aligned} \mathcal{D} &\approx -4s_1 s_2 \omega_c^2 \sin^2 \vartheta_b + m^2 - i\Gamma m \\ &= -4s_1 s_2 \omega_c^2 \sin^2 \vartheta_b + 4s_1 s_2 \omega_r^2 \sin^2 \vartheta_b - i\Gamma m \\ &= -4s_1 s_2 \sin^2 \vartheta_b \left( \omega_c^2 - \omega_r^2 + i \frac{\Gamma m}{4s_1 s_2 \sin^2 \vartheta_b} \right) \\ &\equiv -4s_1 s_2 \sin^2 \vartheta_b (\chi + ia), \end{aligned} \quad (4.43)$$

where

$$\chi \equiv \omega_c^2 - \omega_r^2 = \left(1 - \frac{m^2}{4\omega_1 \omega_2 \sin^2 \vartheta_b}\right) \omega_c^2 \quad (4.44)$$

describes the degrees of deviation of  $E_{cms}$  as determined by a pair of incident photons from the resonance energy derived from the central energy  $\omega_c$ , and  $a$  is defined as

$$a = \frac{\Gamma m \omega_c^2}{4\omega_1 \omega_2 \sin^2 \vartheta_b} = \frac{1}{16\pi} \left(\frac{g}{M}\right)^2 \omega_r^2 m^2. \quad (4.45)$$

The numerator  $\mathcal{N}$  in Eq.(4.39) is considered to be

$$\begin{aligned} \mathcal{N} &= \left(\frac{g}{M}\right)^2 (2\omega_1 \omega_2 \sin^2 \vartheta_b)^2 \\ &= 16\pi a s_1 s_2 \sin^2 \vartheta_b \left(\frac{\omega_c}{\omega_r}\right)^4 \sim 16\pi a s_1 s_2 \sin^2 \vartheta_b, \end{aligned} \quad (4.46)$$

where Eq.(4.41) and (4.45) are used for the second expression and the condition  $\omega_c \sim \omega_r$  is required for the last step because the resonance condition  $E_{cms} = m$  can be satisfied dominantly with a proper choice of  $\vartheta_b$  for a given  $m$  without changing the central beam energy  $\omega_c$  itself. Finally, the following Breit-Wigner distribution is obtained:

$$\mathcal{M}_s = \frac{\mathcal{N}}{\mathcal{D}} = 4\pi \frac{a}{\chi + ia}, \quad \text{and} \quad |\mathcal{M}_s|^2 = (4\pi)^2 \frac{a^2}{\chi^2 + a^2}. \quad (4.47)$$

Since we expect that  $E_{cms}$  is in principle uncertain due to unavoidable energy and momentum uncertainties of a selected pair of two photon wave vectors in QPS, we need to average the resonance effect over a range of  $\chi$ . In order to show the essence of inclusion of an resonance state within a range from  $\chi_-$  to  $\chi_+$ , we demonstrate the simplest averaging as follows. We define  $\chi_{\pm}$  in units of  $a$  as  $\chi_{\pm} = \pm \eta a$  with  $\eta \gg 1$ . The averaging process is expressed as

$$\begin{aligned} \overline{|\mathcal{M}_s|^2} &= \frac{1}{\chi_+ - \chi_-} \int_{\chi_-}^{\chi_+} |\mathcal{M}_s|^2 d\chi \\ &= \frac{(4\pi)^2}{2\eta a} 2a \tan^{-1}(\eta) = (4\pi)^2 \eta^{-1} \tan^{-1}(\eta) \\ &\approx (4\pi)^2 \eta^{-1} \frac{\pi}{2} = 8\pi^2 \frac{a}{|\chi_{\pm}|}, \end{aligned} \quad (4.48)$$

with the approximation due to  $\eta \gg 1$ . Compared to non s-channel cases where  $|\mathcal{M}_s|^2 \propto a^2$ , capturing a resonance within the  $E_{cms}$  uncertainty has a gain of  $a^{-1} \propto M^2$  as shown above. If the energy scale  $M$  corresponds to the Planckian scale  $M_p$ , this gain factor is huge even if we cannot directly capture the top of the Breit-Wigner distribution where  $|\mathcal{M}_s|^2 \propto (4\pi)^2$  with  $\chi \rightarrow 0$ . This is the prominent feature of s-channel scattering including a resonance in QPS. In the following subsections, we will introduce more realistic probability distribution functions for  $E_{cms}$  based on the physical nature of propagating electromagnetic fields in order to implement the averaging process.

#### D. Evaluation of signal yield in stimulated resonant scattering

Let us first consider the number of scattering events in  $p_1 + p_2 \rightarrow p_3 + p_4$  with two colliding photon beams having normalized densities  $\rho_1$  and  $\rho_2$  with average number of photons  $N_1$  and  $N_2$ , respectively. This is referred

to as the *spontaneous* yield to get the signal  $p_3$  in the final state. With the Lorentz-invariant phase space factor  $dL_{ips}$

$$dL_{ips} = (2\pi)^4 \delta(p_3 + p_4 - p_1 - p_2) \frac{d^3 p_3}{2\omega_3 (2\pi)^3} \frac{d^3 p_4}{2\omega_4 (2\pi)^3}, \quad (4.49)$$

the spontaneous signal yield  $\mathcal{Y}$  can be factorized according to the concept of time-integrated luminosity  $\mathcal{L}$  times *cross section*  $\sigma$ , as follows:

$$\begin{aligned} \mathcal{Y} &= N_1 N_2 \left( \int dt d\mathbf{r} \rho_1(\mathbf{r}, t) \rho_2(\mathbf{r}, t) K(p_1, p_2) \right) \times \\ &\quad \left( \frac{c}{2\omega_1 2\omega_2 K(p_1, p_2)} |\mathcal{M}_s(p_1, p_2)|^2 dL_{ips} \right) \\ &\equiv \mathcal{L}(p_1, p_2) [s \cdot L^3 \cdot L^{-3} \cdot L^{-3} \cdot L/s] \sigma(p_1, p_2) [L^2], \end{aligned} \quad (4.50)$$

where  $K$  corresponds to the relative velocity of the incoming particle beams between two incident photons with velocity vectors  $\mathbf{v}_1$  and  $\mathbf{v}_2$ , based on Møller's Lorentz-invariant factor [16]. The relative velocity  $K$  is defined as [17]

$$K(p_1, p_2) \equiv \sqrt{(\mathbf{v}_1 - \mathbf{v}_2)^2 - \frac{(\mathbf{v}_1 \times \mathbf{v}_2)^2}{c^2}} \quad (4.51)$$

with  $c$  the velocity of light. The notation [ ] indicates units with length  $L$  and time  $s$ .

The concept of the *cross section* is convenient for fixed  $p_1$  and  $p_2$  beams. However, in order to implement fluctuations on the velocity vectors, which are represented by the integral on the probability density of cms-energy  $W(Q)$  as a function of the combinations of energies and angles—in laboratory coordinates, denoted as

$$Q \equiv \{\omega_\alpha, \Theta_\alpha, \Phi_\alpha\} \quad \text{and} \quad dQ \equiv \Pi_\alpha d\omega_\alpha d\Theta_\alpha d\Phi_\alpha \quad (4.52)$$

for the incident beams  $\alpha = 1, 2$ —the *volume-wise interaction rate*  $\bar{\Sigma}$  defined below [18] is more straightforward than the *cross section*  $\sigma$

$$\mathcal{Y} = N_1 N_2 \left( \int dt d\mathbf{r} \rho_1(\mathbf{r}, t) \rho_2(\mathbf{r}, t) \right) \times \quad (4.53)$$

$$\begin{aligned} &\left( \int dQ W(Q) \frac{c}{2\omega_1 2\omega_2} |\mathcal{M}_s(Q')|^2 dL'_{ips} \right) \\ &\equiv N_1 N_2 \mathcal{D} [s/L^3] \bar{\Sigma} [L^3/s], \end{aligned} \quad (4.54)$$

because the intermediate  $K$ -factor is canceled in advance of averaging over  $W(Q)$ , where  $Q' \equiv \{\omega_\alpha, \vartheta_\alpha, \phi_\alpha\}$  are kinematical parameters used for the zero- $p_T$  coordinate constructed from a pair of two incident waves. The conversions from  $Q$  to  $Q'$  are possible through rotation functions  $\vartheta_\alpha \equiv \mathcal{R}_{\vartheta_\alpha}(Q)$  and  $\phi_\alpha \equiv \mathcal{R}_{\phi_\alpha}(Q)$ .

We then extend the *spontaneous* yield to the *induced* yield,  $\mathcal{Y}_I$ , by adding one more beam with the central four-momentum  $p_4$  having normalized density  $\rho_4$  with the extended set of parameters:

$$Q_I \equiv \{Q, \omega_4, \Theta_4, \Phi_4\} \quad \text{and} \quad dQ_I \equiv dQ d\omega_4 d\Theta_4 d\Phi_4. \quad (4.55)$$

The induced yield is then expressed as

$$\begin{aligned} \mathcal{Y}_I &= N_1 N_2 N_4 \left( \int dt d\mathbf{r} \rho_1(\mathbf{r}, t) \rho_2(\mathbf{r}, t) \rho_4(\mathbf{r}, t) V_4 \right) \times \\ &\quad \left( \int dQ_I W(Q_I) \frac{c}{2\omega_1 2\omega_2} |\mathcal{M}_s(Q')|^2 dL'_{ips} \right) \\ &\equiv N_1 N_2 N_4 \mathcal{D}_I [s/L^3] \bar{\Sigma}_I [L^3/s], \end{aligned} \quad (4.56)$$

where  $\rho_4(\mathbf{r}, t) V_4$  with the volume of the  $p_4$  beam,  $V_4$ , corresponds to the probability density that describes a spacetime overlap of the  $p_1$  and  $p_2$  beams with the inducing beam  $p_4$ ;  $dL'_{ips}$  indicates the inducible phase space in which the solid angles of  $p_3$  must be consistent so that the balancing solid angles of  $p_4$  determined via energy-momentum conservation can be found within the distribution of the given inducing beam (in laboratory coordinates) after conversion from  $p_4$  in the zero- $p_T$  coordinate system to the corresponding laboratory coordinate.  $W(Q_I)$  is explicitly introduced as

$$W(Q_I) \equiv \Pi_\beta G_E(\omega_\beta) G_p(\Theta_\beta, \Phi_\beta) \quad (4.57)$$

with Gaussian distributions  $G$  for

$$dQ_I \equiv \Pi_\beta d\omega_\beta d\Theta_\beta d\Phi_\beta \quad (4.58)$$

over  $\beta = 1, 2, 4$ . The Gaussian distributions  $G_E$  in the energy space and  $G_p$  in the momentum space (equivalently, the polar angles in the case of photons) are introduced according to the properties of a focused coherent electromagnetic field with an axial symmetric nature for an azimuthal angle  $\Phi$  around the optical axis of a focused beam, as we discuss soon.

We then specifically consider a search for signal photons  $p_3$  for the degenerate case in the generic QPS including asymmetric collisions:  $p_c + p_c \rightarrow p_3 + p_4$  where  $p_1$  and  $p_2$  are stochastically obtained from a single focused coherent beam with central photon energy  $\omega_c$  under the co-propagating focused coherent beam with central four-momentum  $p_4$  for the purpose of induction. Based on the transition amplitude in Eq.(4.28) and the yield expression in Eq.(4.56), the induced signal yield in the degenerate case, where we combine a coherent creation beam and a coherent inducing beam with the average numbers of photons  $N_c$  and  $N_i$ , respectively, and focus them into the common optical axis (in laboratory coordinates) is expressed as

$$\mathcal{Y}_{c+i} = (N_c/2)(N_c/2)N_i \times \quad (4.59)$$

$$\begin{aligned} &\left( \int dt d\mathbf{r} \rho_c(\mathbf{r}, t) \rho_c(\mathbf{r}, t) \rho_i(\mathbf{r}, t) V_i \right) \times \\ &\left( \int dQ_I W(Q_I) \frac{c}{2\omega_1 2\omega_2} |\mathcal{M}_s(Q')|^2 dL'_{ips} \right) \\ &\equiv \frac{1}{4} N_c^2 N_i \mathcal{D}_I [s/L^3] \bar{\Sigma}_I [L^3/s], \end{aligned}$$

where the factor 1/4 appears for the reason explained in the paragraph just below Eq.(4.28) and  $\mathcal{M}_S$  is based on the non-degenerate case resulting in Eq.(4.39). In the following, we provide detailed formulas for  $\mathcal{D}_I$  and  $\bar{\Sigma}_I$  in Eq.(4.59).

### 1. Properties of a Gaussian beam in vacuum

The solution for propagation of an electromagnetic field in vacuum is known as the basic Gaussian mode [20]. In the Gaussian mode, the electric field propagating along the  $z$ -direction with wave number  $k$  in (laboratory) spatial coordinates  $(x, y, z)$  is expressed as

$$\mathbf{E}(x, y, z) = \mathbf{E}_0 \frac{w_0}{w(z)} \times \exp\left(-i(kz - \eta(z)) - r^2 \left(\frac{1}{w^2(z)} + \frac{ik}{2R(z)}\right)\right), \quad (4.60)$$

where the individual factors are summarized as follows.

$$\begin{aligned} r &= \sqrt{x^2 + y^2} \\ w(z) &= w_0 \sqrt{1 + \frac{z^2}{z_R^2}} \\ \eta(z) &= \tan^{-1}\left(\frac{z}{z_R}\right) \\ R(z) &= z \left(1 + \frac{z_R^2}{z^2}\right) \end{aligned} \quad (4.61)$$

In this, the beam waist  $w_0$  and Rayleigh length  $z_R$  are

$$w_0 = \frac{\lambda}{\pi\vartheta_0}, \quad z_R = \frac{\pi w_0^2}{\lambda} \quad (4.62)$$

for a given wavelength  $\lambda$ . When a single electromagnetic field is focused with focal length  $f$  and beam diameter  $d$ , the beam waist is related to the incident angle  $\Theta_0$  by

$$\Theta_0 = \tan^{-1}\left(\frac{d}{2f}\right). \quad (4.63)$$

At the focal point  $z = 0$ , the spatial distribution of the electric field is expressed as

$$\mathbf{E}(x, y, z = 0) = \mathbf{E}_0 \exp\left(-\frac{x^2 + y^2}{w_0^2}\right). \quad (4.64)$$

The corresponding wave number distribution is obtained by Fourier transformation of the electric field, yielding

$$\begin{aligned} \hat{\mathbf{E}}(k_x, k_y, 0) &= \frac{1}{4\pi^2} \int_{-\infty}^{\infty} \mathbf{E}_0 \exp\left(-\frac{x^2 + y^2}{w_0^2}\right) \times \\ &\exp(-i(k_x x + k_y y)) dx dy = \frac{w_0^2 \mathbf{E}_0}{4\pi} \exp\left(-\frac{w_0^2}{4}(k_x^2 + k_y^2)\right). \end{aligned} \quad (4.65)$$

The uncertainty on incident angles of wave vectors within the electric field with respect to the  $z$ -axis can be related to  $k_T = \sqrt{k_x^2 + k_y^2}$  via the variance

$$\sigma_{k_T}^2 = \frac{2}{w_0^2} \quad (4.66)$$

in the Gaussian form.

For incident angles  $\Theta$  defined with the transverse momenta  $k_T$  in Eq.(4.66) and the incident energies  $\omega$  with  $\hbar = 1$ ,

$$\Theta = \sin^{-1}\left(\frac{k_T}{\omega}\right), \quad (4.67)$$

and the error propagation on the incident angles is given by

$$\begin{aligned} \sigma_\Theta &= \sqrt{\left(\frac{\partial\Theta}{\partial k_T}\right)^2 \sigma_{k_T}^2 + \left(\frac{\partial\Theta}{\partial\omega}\right)^2 \sigma_\omega^2} \\ &= \sqrt{\frac{1}{\langle\omega\rangle^2 - \langle k_T\rangle^2} \left(\sigma_{k_T}^2 + \left(\frac{\langle k_T\rangle}{\langle\omega\rangle}\right)^2 \sigma_\omega^2\right)} \\ &= \frac{1}{\omega_c} \sigma_{k_T} = \frac{1}{\sqrt{2}} \Theta_0, \end{aligned} \quad (4.68)$$

where  $\langle\omega\rangle = \omega_c$ ,  $\langle k_T\rangle = 0$ , and Eq.(4.66) are substituted for the last line.

The average number of photons,  $N$ , in a pulsed electromagnetic field can be related to the square of the electric field,  $I$ , by adding a Gaussian-shaped time distribution with duration  $\tau$ , as follows:

$$I(t, x^i) = E_0^2 \frac{w_0^2}{w^2(ct)} \exp\left(-2\frac{x^2 + y^2}{w^2(ct)}\right) \exp\left(-2\left(\frac{z - ct}{c\tau}\right)^2\right), \quad (4.69)$$

where  $E_0^2$  corresponds to  $N$ . The volume for the normalization is then expressed as

$$V = \int_{-\infty}^{\infty} dx^i \frac{I}{E_0^2} = \left(\frac{\pi}{2}\right)^{\frac{3}{2}} w_0^2 c\tau. \quad (4.70)$$

Therefore, the normalized density profile per photon,  $\rho \equiv I/(NV)$ , is expressed as

$$\rho(t, x^i) = \frac{(2/\pi)^{3/2}}{w^2(ct)c\tau} \exp\left(-2\frac{x^2 + y^2}{w^2(ct)}\right) \exp\left(-2\left(\frac{z - ct}{c\tau}\right)^2\right). \quad (4.71)$$

### 2. Integrated inducible volume-wise interaction rate, $\bar{\Sigma}_I$

With the kinematical parameters defined in a zero- $p_T$  coordinate as illustrated in Fig.4,  $Q' \equiv \{\omega_1, \omega_2, \vartheta_1, \vartheta_2, \phi_1, \phi_2\}$ , we first discuss the integrand of the spontaneous volume-wise interaction rate in Eq.(4.53) in individual zero- $p_T$  coordinates

$$\Sigma' \equiv \frac{c}{2\omega_1 2\omega_2} |\mathcal{M}_s(Q')|^2 dL'_{ips}. \quad (4.72)$$

With  $d^3p_3 = \omega_3^2 d\omega_3 d\Omega'_3$ , the differential volume-wise interaction rate per solid angle  $d\Omega'_3$  in a zero- $p_T$  coordinate

is expressed as

$$\frac{d\Sigma'}{d\Omega_3'} = \frac{c}{32\pi^2\omega_1\omega_2} \int_0^\infty d\omega_3\omega_3 \times \int_{-\infty}^\infty d^3p_4 \frac{|\mathcal{M}_s(Q')|^2}{2\omega_4} \delta^4(p_3 + p_4 - p_1 - p_2). \quad (4.73)$$

We then insert the following identity

$$1 = \int_0^\infty dp_4^0 \delta(p_4^0 - \omega_4) = \int_{-\infty}^\infty dp_4^0 2\omega_4 \delta(p_4^2) \Theta(p_4^0) \quad (4.74)$$

to derive

$$\begin{aligned} & \int \frac{d^3p_4}{2\omega_4} \delta^4(p_3 + p_4 - p_1 - p_2) \\ &= \int d^4p_4 \delta(p_4^2) \Theta(p_4^0) \delta^4(p_3 + p_4 - p_1 - p_2) \\ &= \delta((p_1 + p_2 - p_3)^2), \end{aligned} \quad (4.75)$$

where  $\omega_4 > 0$  is guaranteed. In an asymmetric QPS, the following relation holds due to energy-momentum conservation:

$$\begin{aligned} p_4^2 &= (p_1 + p_2 - p_3)^2 \\ &= 2(\omega_1 + \omega_2 - \omega_z \cos \vartheta_3) \left( \omega_3 - \frac{2\omega_1\omega_2 \sin^2 \vartheta_b}{\omega_1 + \omega_2 - \omega_z \cos \vartheta_3} \right). \end{aligned} \quad (4.76)$$

Hence,

$$\begin{aligned} \delta(p_4^2) &= \frac{1}{2(\omega_1 + \omega_2 - \omega_z \cos \vartheta_3)} \delta(\omega_3 - \hat{\omega}_3) \\ &= \frac{\hat{\omega}_3}{4\omega_1\omega_2 \sin^2 \vartheta_b} \delta(\omega_3 - \hat{\omega}_3), \end{aligned} \quad (4.77)$$

where

$$\hat{\omega}_3 \equiv \frac{2\omega_1\omega_2 \sin^2 \vartheta_b}{\omega_1 + \omega_2 - \omega_z \cos \vartheta_3}. \quad (4.78)$$

Therefore, we can write the expression

$$\begin{aligned} \frac{d\Sigma'}{d\Omega_3'} &= \frac{c}{32\pi^2\omega_1\omega_2} \times \\ & \int_0^\infty d\omega_3\omega_3 \frac{\hat{\omega}_3}{4\omega_1\omega_2 \sin^2 \vartheta_b} |\mathcal{M}_s(Q')|^2 \delta(\omega_3 - \hat{\omega}_3) \\ &= \frac{c\hat{\omega}_3^2 |\mathcal{M}_s(Q')|^2}{2(8\pi\omega_1\omega_2 \sin \vartheta_b)^2}. \end{aligned} \quad (4.79)$$

Because the incident energies and momenta fluctuate for the single creation beam, the differential volume-wise interaction rate must be averaged over possible values of  $\chi$  in Eq.(4.44) according to the probability distribution functions  $W(Q) \equiv G_E(\omega_1)G_E(\omega_2)G_p(\Theta_1, \Phi_1)G_p(\Theta_2, \Phi_2)$  with the parameters in laboratory coordinates, where

$$G_E(\omega) \equiv \frac{1}{\sqrt{2\pi}\sigma_\omega} \exp\left(-\frac{(\omega - \bar{\omega})^2}{2\sigma_\omega^2}\right), \quad (4.80)$$

with mean  $\bar{\omega}$  and

$$G_p(\Theta, \Phi) \equiv \frac{1}{2\pi\sigma_\Theta^2} \exp\left(-\frac{\Theta^2}{2\sigma_\Theta^2}\right) = \frac{1}{\pi\Theta_0^2} \exp\left(-\frac{\Theta^2}{\Theta_0^2}\right) \quad (4.81)$$

by substituting  $\sigma_\Theta = \Theta_0/\sqrt{2}$  from Eq.(4.68) for the second. We note that  $G_p$  is normalized to the two-dimensional Gaussian distribution in  $\Theta - \Phi$  angular space, where the  $\Phi$ -dependence is implicitly implemented via the axial symmetric feature of a focused beam even though the right-hand side includes only the  $\Theta$ -dependence. With the explicit notation  $dQ \equiv d\omega_1 d\omega_2 d\Theta_1 d\Theta_2 d\Phi_1 d\Phi_2$ , the integrated differential volume-wise interaction rate in the zero- $p_T$  coordinate is then expressed as

$$\frac{d\bar{\Sigma}'}{d\Omega_3} \equiv \int dQ W(Q) \frac{c|\mathcal{M}_s(\mathcal{R}(Q))|^2}{2(8\pi\omega_1\omega_2 \sin \vartheta_b)^2}, \quad (4.82)$$

where  $\mathcal{R}$  denotes rotation functions that convert a  $Q$  given in laboratory coordinates to  $Q'$  in the corresponding zero- $p_T$  coordinate system.

So far, we have discussed the spontaneous scattering process resulting in the two-photon final state with  $p_3$  and  $p_4$ . We now discuss the stimulated volume-wise interaction rate with a coherent inducing field at the space-time where the scattering takes place. We then need to revisit the commutation relation used in Eq.(4.11). To have the enhancement factor  $\sqrt{N_{p_4}}$  appear through the second relation in Eq.(4.18), both momentum and polarization states of the spontaneous  $p_4$ -wave must be identical with those in the inducing coherent field. As for the matching of polarization state, as long as we consider circular polarization states (for instance,  $S = LLRR$ ), the matching is satisfied for any directions of  $p_4$ -waves in the inducing beam with the  $R$ -state resulting in a  $p_3$ -wave with an  $R$ -state. On the other hand, for the momentum state matching, we need to evaluate what fraction of the inducing beam can actually stimulate the scattering process; that is, the enhancement factor possible for the coherent state, because the focused short-pulse inducing beam has a spread in both momentum and energy spaces. Phase-space matching can be implemented by introducing the symbol  $dL'_{ips}$ . This symbol indicates that we take into account the solid angles of signal photons,  $p_3$ , only when we can find balancing  $p_4$  waves via energy-momentum conservation within the given focused inducing field. More explicitly, we define the following relation:

$$\begin{aligned} \bar{\Sigma}_I &\equiv \int G_E(\omega_4) G_p(\Theta_4, \Phi_4) d\Omega_4 \times \\ & \frac{d\Omega_4'}{d\Omega_4} \frac{d\Omega_3'}{d\Omega_4'} \frac{d\bar{\Sigma}'}{d\Omega_3'}, \end{aligned} \quad (4.83)$$

where

$$\frac{d\Omega_3'}{d\Omega_4'} = \frac{d\phi_3 \sin \vartheta_3}{d\phi_4 \sin \vartheta_4} \frac{d\vartheta_3}{d\vartheta_4} = \frac{\sin \vartheta_3}{\sin \vartheta_4} \frac{d\vartheta_3}{d\vartheta_4} = -\left(\frac{\omega_4}{\omega_3}\right)^2 \quad (4.84)$$

This is based on the energy-momentum conservation in Eq.(4.31) and  $d\phi_3 = d\phi_4$  in zero- $p_T$  coordinates. Because an inducible solid angle of  $p_4$  in a zero- $p_T$  coordinate must match with a solid angle within the angular distribution of the inducing coherent field mapped in laboratory coordinates,  $d\Omega_4 = d\Omega'_4$  must be satisfied. Therefore, the inducible volume-wise interaction rate is eventually expressed as

$$\begin{aligned} \bar{\Sigma}_I &= - \int G_E(\omega_4) G_p(\Theta_4, \Phi_4) d\Omega_4 \left( \frac{\omega_4}{\omega_3} \right)^2 \frac{d\bar{\Sigma}'}{d\Omega_3} \quad (4.85) \\ &= \int_0^{2\pi} d\Phi_4 \int_{\pi/2}^0 d\Theta_4 \sin \Theta_4 G_p(\Theta_4, \Phi_4) \times \\ &\quad \int d\omega_4 G_E(\omega_4) \left( \frac{\omega_4}{\omega_1 + \omega_2 - \omega_4} \right)^2 \times \\ &\quad \int dQ W(Q) \frac{c |\mathcal{M}_s(\mathcal{R}(Q))|^2}{2(8\pi\omega_1\omega_2 \sin \vartheta_b)^2}, \end{aligned}$$

where all integral variables are expressed by those defined in the laboratory coordinate,  $Q_I$  as defined in Eq.(4.55) that includes  $Q$  in Eq.(4.52).

### 3. Spacetime overlapping factor with an inducing beam, $\mathcal{D}_I$

For scattering in QPS, we introduce a common normalized density for the incident beams as  $\rho_c \equiv \rho_1 = \rho_2$  by assuming that  $p_1$  and  $p_2$  are stochastically selected from the single creation beam and the inducing beam  $\rho_i$  based on Eq.(4.71) as follows:

$$\begin{aligned} \rho_c(t, x^i) &= \left( \frac{2}{\pi} \right)^{\frac{3}{2}} \frac{1}{w_c^2(ct) c\tau_c} \times \quad (4.86) \\ &\quad \exp \left( -2 \frac{x^2 + y^2}{w_c^2(ct)} \right) \exp \left( -2 \left( \frac{z - ct}{c\tau_c} \right)^2 \right) \end{aligned}$$

$$\begin{aligned} \rho_i(t, x^i) &= \left( \frac{2}{\pi} \right)^{\frac{3}{2}} \frac{1}{w_i^2(ct) c\tau_i} \times \quad (4.87) \\ &\quad \exp \left( -2 \frac{x^2 + y^2}{w_i^2(ct)} \right) \exp \left( -2 \left( \frac{z - ct}{c\tau_i} \right)^2 \right), \end{aligned}$$

where the origin is defined at  $t = 0$  and  $x^i = 0$  for  $i = 1 - 3$ , and the pulse durations  $\tau_c$  and  $\tau_i$  follow independent Gaussian distributions. Because we discussed the angular spread only at the origin in Eq.(4.65), where the maximum interaction rate is expected, we limit the region of interest to within the Rayleigh length  $z_R$  in order to provide a conservative estimate of the yield. Therefore, with  $V_i = (\pi/2)^{3/2} w_{i0}^2 c\tau_i$  from Eq.(4.70), the overlap factor is approximated as

$$\begin{aligned} \mathcal{D}_I &\approx \int_{-z_R/c}^0 dt \int_{-\infty}^{\infty} dx^i \rho_c^2(t, x^i) \rho_i(t, x^i) V_i \quad (4.88) \\ &= \left( \frac{2}{\pi} \right)^{\frac{3}{2}} \frac{1}{c} \frac{\tau_i}{\tau_c} \frac{1}{\sqrt{\tau_c^2 + 2\tau_i^2}} w_{i0}^2 \times \\ &\quad \int_{-z_R/c}^0 dt \frac{1}{w_c^4(ct) + 2w_c^2(ct)w_i^2(ct)}, \end{aligned}$$

where the integrand

$$\frac{A}{w_c^2(ct)} - \frac{B}{w_c^2(ct) + 2w_i^2(ct)}$$

with

$$A = \frac{1}{2w_{i0}^2 \left\{ 1 - \left( \frac{z_{cR}}{z_{iR}} \right)^2 \right\}}$$

and

$$B = \frac{1}{1 - \left( \frac{z_{cR}}{z_{iR}} \right)^2} \left\{ \frac{1}{2w_{i0}^2} + \frac{1}{w_{c0}^2} \left( \frac{z_{cR}}{z_{iR}} \right)^2 \right\}.$$

Finally, the spacetime overlap factor for the two effective beams in QPS is expressed as

$$\begin{aligned} \mathcal{D}_I &\approx \sqrt{\frac{2}{\pi}} \frac{1}{c^2} \frac{\tau_i}{\tau_c} \frac{1}{\sqrt{\tau_c^2 + 2\tau_i^2}} \frac{\lambda_i^2}{\lambda_i^2 - \lambda_c^2} \times \quad (4.89) \\ &\quad \left[ \frac{1}{\lambda_c} \tan^{-1} \left( \frac{\lambda}{\lambda_c} \right) - \frac{1}{\lambda_{ci}} \tan^{-1} \left( \frac{\lambda}{\lambda_{ci}} \right) \right] \end{aligned}$$

with  $\lambda_{ci} \equiv \sqrt{\frac{\lambda_c^2 + 2\lambda_i^2}{3}}$ .